NJC

Cite this: *New J. Chem.*, 2011, **35**, 2781–2792

www.rsc.org/njc

PAPER

Synthesis, thermal stability and photoresponsive behaviors of azobenzene-tethered polyhedral oligomeric silsesquioxanes†

Jinlan Zhou,[a] Yongchen Zhao,[a] Kaichao Yu,[a] Xingping Zhou*[a] and Xiaolin Xie[ab]

Received (in Montpellier, France) 4th July 2011, Accepted 8th September 2011
DOI: 10.1039/c1nj20577c

A series of azobenzene-tethered polyhedral oligomeric silsesquioxane (POSS) derivatives, *i.e.* monoazobenzene-substituted POSS (**MonoAzo-POSS**), bisazobenzene-substituted POSS (**BisAzo-POSS**) and triazobenzene-substituted POSS (**TriAzo-POSS**), were synthesized through the amidation acidylation of aminopropylisobutyl POSS and benzoic acid derivatives (**AzoM**s) with one, two and three azobenzene groups (**AzoM1**, **AzoM2** and **AzoM3**). Their structures were characterized by FT-IR, ^{1}H NMR, ^{13}C NMR and mass spectra, and their thermal stability and photoresponsive behaviors in DMF solutions were evaluated with TGA, XRD and UV-vis spectra, respectively. The results indicated that the thermal stability and photoisomerization of azobenzenes could be effectively controlled by their molecular structure. In **MonoAzo-POSS**, the large steric hindrance of POSS destroys the molecular ordering and limits the molecular packing, contributing to its poor thermal stability. And the low molecular ordering of **MonoAzo-POSS** offers an azo group with large free space, and its *trans–cis* photoisomerization rate increases accordingly. But, in **BisAzo-POSS** and **TriAzo-POSS**, the incorporation of POSS units does not impact on the regularity of azobenzenes obviously, and the hindrance effect of nanosize POSS on the molecular motion plays a primary role in increasing their high thermal stability. Their photoisomerization rates decrease due to the steric hindrance of POSS and the unfolding structure of the azo moieties in **BisAzo-POSS** and **TriAzo-POSS**.

1. Introduction

Photoresponsive molecular materials with azobenzene (Azo) units are promising for applications such as photochemical switches,[1,2] optical information data-storages,[3,4] sensors,[5] liquid crystal display,[6] optical limiting,[7,8] site-related drug release,[9] and light-driven machines or actuators.[10–12] For high performance devices, the used materials require high thermal stability, low fatigue, rapid response, high sensitivity, and excellent processability. Mita *et al.*[2] prepared polycarbonate/azobenzene composite films and investigated their photoisomerization. They found that the azobenzene in polycarbonate at room temperature has the same *trans–cis* photoisomerization rate as in ethyl acetate and ethanol up to a conversion less than 86%, and then the *trans–cis* photoisomerization deviates from the first-order kinetics due to the effect of free volume distribution on the reactivity of azobenzene in polycarbonate. Sasaki *et al.*[13] studied the photoisomerization and thermal isomerization behaviors of azobenzenes in nematic and smectic polymer liquid crystals (PLCs), and found that the azobenzenes show faster photoisomerization in the former than in the latter since the nematic matrix possesses more inner free volume than the smectic one. In order to enhance the dispersion of azobenzene in the polymer matrix, the azobenzene units are usually bonded in the polymer chains or attached on the side chains covalently.[4] However, the thermo- and photo-stability of those materials are not enough at higher temperatures due to the rotational freedom of the chromophores and the motion of polymer chains.[7] Recently, azobenzene chromophores have been incorporated into the inorganic silica network by the sol–gel process,[14,15] the formed organic–inorganic hybrid materials show good thermal stability, excellent nonlinear optical properties, and reversible photoisomerization. But the sol–gel glass film is more rigid, and there exists a strong interaction between its precursor tetraethyl orthosilicate (TEOS) and azobenzene, leading to the partial suppression of the isomerization of azobenzene.[16]

Polyhedral oligomeric silsesquioxane (POSS) is a unique modifier to high-performance materials due to its unique three-dimensional structure.[17,18] In POSS molecules, the rigid

[a] *Hubei Key Laboratory of Materials Chemistry and Service Failure, School of Chemistry and Chemical Engineering, Huazhong University of Science and Technology, Wuhan, 430074, China. E-mail: xpzhou@mail.hust.edu.cn; Fax: +86-27-8754-3632; Tel: +86-27-8755-8194*
[b] *National Anti-counterfeit Engineering Research Center, Huazhong University of Science and Technology, Wuhan, 430074, China*

† Electronic supplementary information (ESI) available: Experimental details, FTIR, ^{1}H NMR and Raman spectra. See DOI: 10.1039/c1nj20577c

inorganic core provides high stiffness, thermo- and photostability, the organic corner groups offer excellent solubility, processability and compatibility with other materials. Many POSS-based functional materials, such as liquid crystal (LC) materials,[19–22] light-emitting materials,[23–25] dental restorative materials[26] and ionic liquid,[27] have been prepared. And they are usually based on mono- or octa-substituted POSSs. The incorporation of POSS moieties into organic molecules or polymers may have dramatic effects on their properties, these hybrid materials display superior properties to the organic material alone. Thermal stability and photoresponsive behaviors of azobenzene compounds depend strongly on their structure and size, but the effect of the molecular regularity on properties of POSS-based azobenzene hybrids has not been found. In order to explore the relationship of the molecular structure and its thermostability, photoisomerization and potential application in optical data storage and optical switches, we first designed and synthesized a series of azobenzene-tethered POSS derivatives (**Azo-POSS**s), *i.e.* monoazobenzene substituted POSS (**MonoAzo-POSS**), bisazobenzene substituted POSS (**BisAzo-POSS**) and triazobenzene substituted POSS (**TriAzo-POSS**), as shown in Fig. 1, and then studied their thermal stability and photoresponsive behaviors.

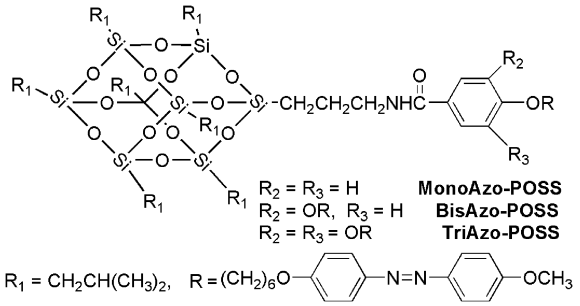

Fig. 1 Chemical structures of **MonoAzo-POSS**, **BisAzo-POSS** and **TriAzo-POSS**.

2. Results and discussion

2.1 Synthesis and structure of AzoMs and their hybrids with POSS

AzoMs, **NH_2-POSS** and **Azo-POSS**s were successfully synthesized according to the procedures in Scheme 1. Azobenzene monomers (**AzoM**s), including 4-(6-(4-(4-methoxy)phenylazo)-phenoxy) hexyloxybenzoic acid (designated as **AzoM1**), 3,4-bis (6-(4-(4-methoxy)phenylazo)phenoxy)hexyloxybenzoic acid (designated as **AzoM2**), and 3,4,5-tri(6-(4-(4-methoxy)-phenylazo)phenoxy)hexyloxybenzoic acid (designated as **AzoM3**), were synthesized by a substitution reaction of 1-bromo-6-(4-methoxyazobenzene-4′-oxy) hexane (**BrMAB**) with methyl-4-hydroxybenzoate, methyl-3,4-dihydroxybenzoate and methyl-3,4,5-trihydroxy-benzoate, respectively. Synthetic procedures of **BrMAB** were reported by Mitsuoka *et al.* and Yang *et al.*[28,29] However, the shortcomings include the requirement for recrystallization and relatively low yield (from 46% to 52%) making them inefficient in preparing **BrMAB**. In this work, **BrMAB** was prepared efficiently by prolonging the time for alkylation reaction of 4-hydroxy-4′-methoxyazobenzene (**HMAB**) with 1,6-dibromohexane from 24 h to 36 h and changing purification procedures. Compared with the previous methods, our method not only gives a higher

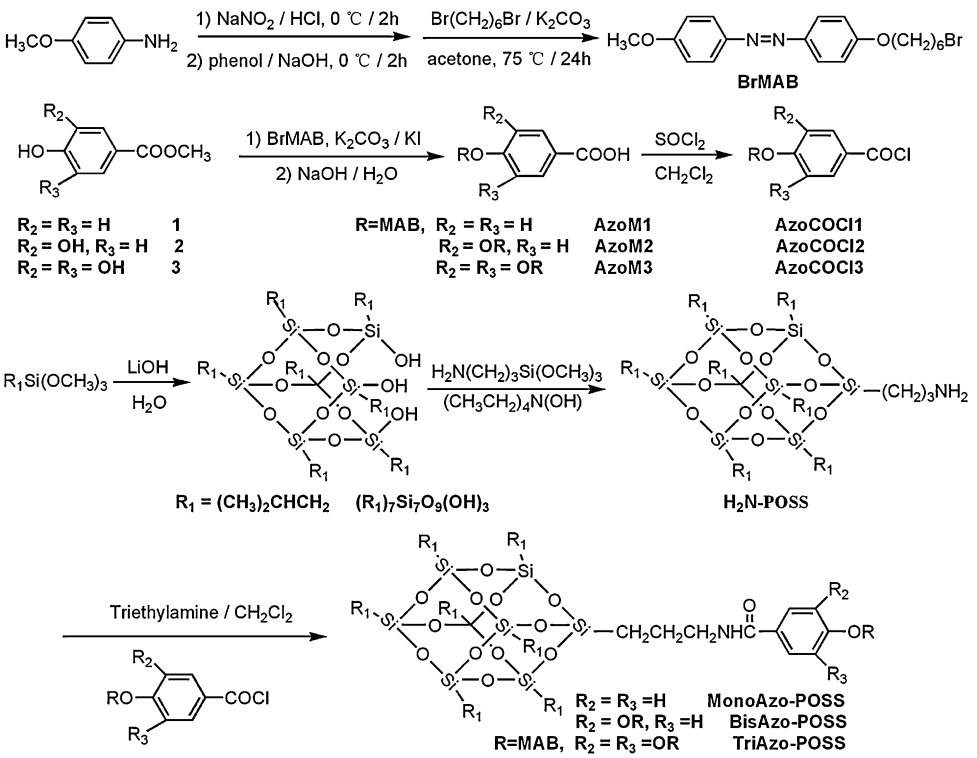

Scheme 1 Synthetic procedures of **AzoM**s, **NH_2-POSS** and **Azo-POSS**s.

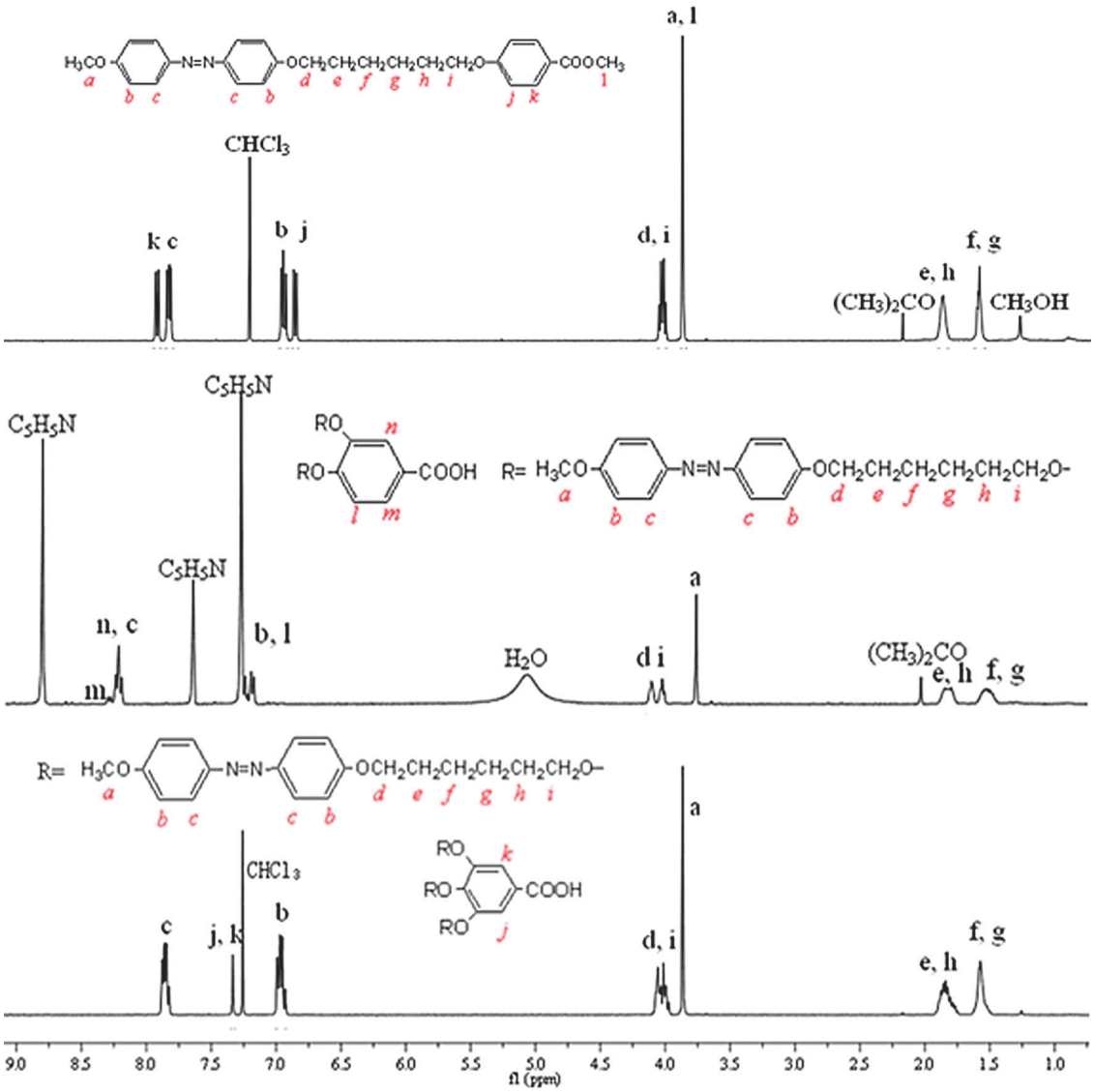

Fig. 2 ^{1}H NMR spectra of **AzoM2**, **AzoM3** and ester of **AzoM1**.

yield (70%), but also offers attractive features such as operational convenience, dispensing with the recrystallization process.

From ^{1}H NMR spectra of **AzoM2**, **AzoM3** and methyl-4-(6-(4-(4-methoxy)phenylazo)phenoxy)hexyloxybenzoate (ester of **AzoM1**) (Fig. 2), there exists a singlet peak at 3.75–3.87 ppm (–OCH_3 on the aromatic rings), multiplet peaks at 6.95–8.2 ppm (Ar–*H*), triplet peaks at 3.95–4.08 ppm (–OCH_2– on the aromatic rings) and multiplet peaks at 1.48–1.90 ppm (–CH_2CH_2–) with the ratio of the integrated areas of the absorption peaks in accordance with the proton number of the expected compounds, respectively. These details and FT-IR spectra are given in ESI.† It is worth noting that no NMR spectrum of **AzoM1** was recorded due to its poor solubility in ordinary solvents, such as $CDCl_3$, CD_3OD, $(CD_3)_2CO$ and DMSO. These results indicate that **AzoM**s are consistent with the proposed chemical structures.

As shown in Scheme 1, three kinds of azobenzene-tethered POSSs, *i.e.* (*N*-(3-(3,5,7,9,11,13,15-heptaisobutyl)pentacyclo[9,5,1,1^{3,9},1,^{7,13}1^{5,15}]octasiloxane-1-yl)-propyl-4-(6-(4-(4-methoxy)phenylazo)phenoxy)hexyloxybenzamide) (**MonoAzo-POSS**), (*N*-(3-(3,5,7,9,11,13,15-hepta-isobutyl)pentacyclo-[9,5,1,1^{3,9},1,^{7,13}1^{5,15}]octasiloxane-1-yl)-propyl-3,4-bis(6-(4-(4-methoxy)phenylazo)phenoxy)hexyloxybenzamide) (**BisAzo-POSS**) and (*N*-(3-(3,5,7,9,11,13,15-hepta-isobutyl)pentacyclo-[9,5,1,1^{3,9},1,^{7,13}1^{5,15}]octasiloxane-1-yl)-propyl-3,4,5-tri(6-(4-(4-methoxy)-phenylazo)phenoxy)hexyloxybenzamide) (**TriAzo-POSS**) were synthesized by reaction of 3-(3,5,7,9,11,13,15-heptaisobutylpentacyclo[9,5,1,1,^{3,9}1,^{7,13}1,^{5,15}]octasiloxane-1-yl)-propylamine (**NH$_2$-POSS**) with the acyl chlorides of **AzoM**s.

The starting compound for **NH$_2$-POSS** was prepared *via* catalytic hydrolysis and condensation of isobutyltrimethoxysilane to yield incompletely condensed 1,3,5,7,9,11,14-heptaisobutyltricyclo[7,3,3,1^{5,14}]heptasiloxane-3,7,11-trisilanol (**trisilanolisobutyl-POSS**) in the presence of lithium hydroxide, and then corner-capping reaction between **trisilanolisobutyl-POSS** and 3-aminopropyltrimethoxysilane was employed to obtain **NH$_2$-POSS**.[30,31]

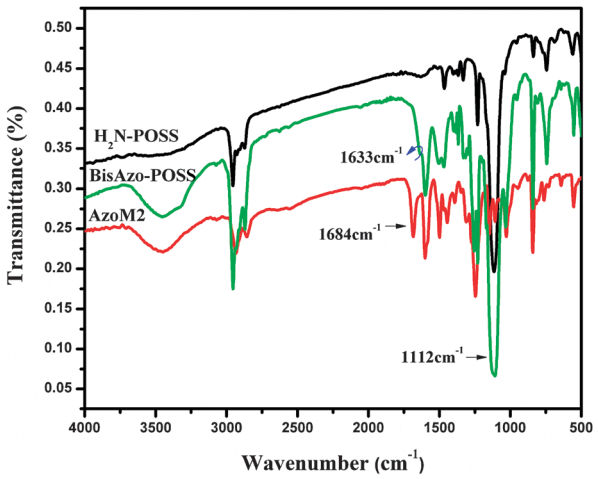

Fig. 3 FT-IR spectra of **NH_2-POSS**, **BisAzo-POSS** and **AzoM2**.

Fig. 3 shows FT-IR spectra of **NH_2-POSS**, **BisAzo-POSS** and **AzoM2**, the typical υ (Si–O) strong bands at about 1112 cm^{-1} and characteristic bands between 2873 and 2956 cm^{-1} are due to the vibration frequency of the C–H bond. The characteristic absorption bands in **AzoM2** are located at ~3448 cm^{-1} for υ (O–H), 1467 and 1601 cm^{-1} for υ (aromatic ring) and 1684 cm^{-1} for υ (C=O), respectively. Especially, the absorption band at 1633 cm^{-1} is due to carbonyl stretching vibration (amide I) in **BisAzo-POSS**. This proves that **AzoM2** was anchored onto the POSS, and FT-IR spectra of other **Azo-POSS**s are provided in ESI.†

Fig. 4 shows ^{1}H NMR spectra of **MonoAzo-POSS**, **BisAzo-POSS** and **TriAzo-POSS**. For example, the ^{1}H NMR spectrum of **BisAzo-POSS** is composed of the resonance peaks of the protons, such as aromatic rings δ (ppm): 6.97 (dd, Ar–*H*, 8H), 7.84 (m, Ar–*H*, 8H), 6.97 (dd, Ar–*H*, 8H), 7.84 (m, Ar–*H*, 8H), 6.83 (dd, Ar–*H*, 1H) and 7.42 (dd, Ar–*H*, 1H), aliphatic hydrocarbon groups δ (ppm): 3.84 (s, –OCH_3, 6H), 4.03 (t, –OCH_2–, 8H), 1.83 (m, –OCH$_2CH_2$–, –SiCH$_2CH$, 15H), 1.58 (m, –CH_2CH_2–, 8H), 3.42 (t, –NHCH_2, 2H), 1.71 (m, –NHCH$_2CH_2$, 2H), 0.63 (m, –SiCH_2CH$_2$, 2H), 0.59 (m, –SiCH_2CH, 14H), 0.98 (D, –CH(CH_3)$_2$, 42H), and amide group δ (ppm): 5.99 (s, *NH*, 1H). Additionally, in terms of the integration intensities of protons in the aliphatic methyl,

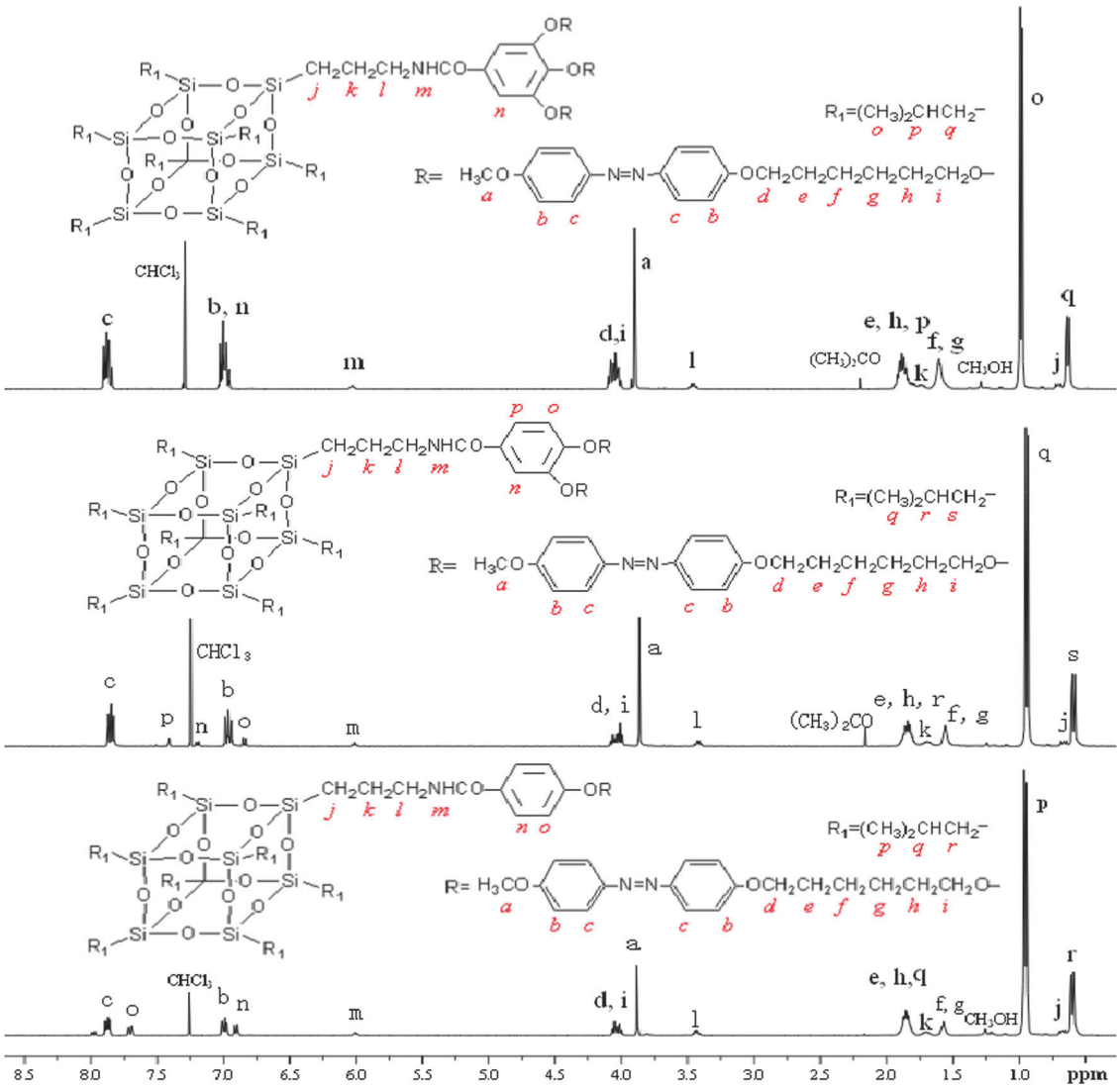

Fig. 4 ^{1}H NMR spectra of **MonoAzo-POSS**, **BisAzo-POSS** and **TriAzo-POSS**.

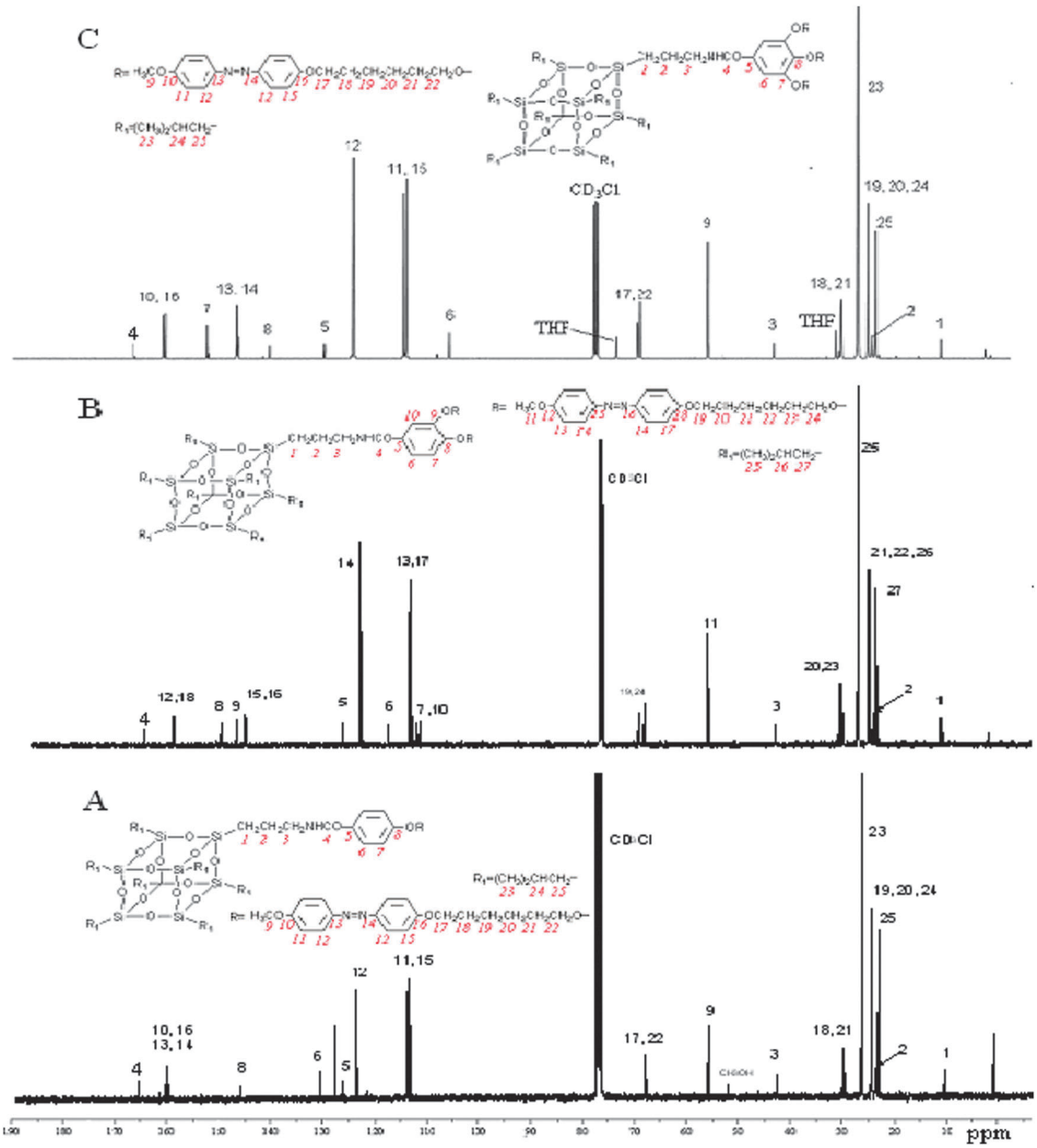

Fig. 5 ^{13}C NMR spectra of **MonoAzo-POSS**, **BisAzo-POSS** and **TriAzo-POSS**.

methylene and methenyl moiety to protons of aromatic rings, it can be judged that the POSS compounds possess one propyl group, seven isobutyl groups and one **AzoM2** group. ^{1}H NMR spectra of **MonoAzo-POSS** and **TriAzo-POSS** are similar to that of **BisAzo-POSS**.

Fig. 5 shows ^{13}C NMR spectra of **MonoAzo-POSS**, **BisAzo-POSS** and **TriAzo-POSS**. For example, the characteristic C═O signal is observed at 167.07 ppm in **BisAzo-POSS**, the peaks at 114.65, 114.15, 124.34, 146.98, 146.95, 161.54, 161.15, 119.15, 112.3,151.74, 149.00, 113.01, 127.60 ppm are assigned to aromatic carbons, and all kinds of aliphatic carbon peaks are observed at 42.32, 25.82, 23.85, 23.15, 22.48, 9.53, 55.50, 68.98, 68.14, 29.69, 29.10 ppm. Also, ^{13}C NMR spectra of **MonoAzo-POSS** and **TriAzo-POSS** are similar to that of **BisAzo-POSS**. Detail data are shown in ESI.†

Furthermore, their ESI-HRMS and FAB-MS are as follows: FAB-MS for **MonoAzo-POSS**, *m*/*z*, calcd $C_{57}H_{98}N_3Si_8O_{16}$ ($[M + H]^+$): 1304.51 found: 1304.7; HRMS-MS for **BisAzo-POSS**, calcd $C_{76}H_{119}N_5Si_8O_{19}Na$ ($[M + Na]^+$): 1653.6566, found: 1653.6621; HRMS-MS for **TriAzo-POSS** calcd $C_{95}H_{141}N_7Si_8O_{22}Na$ ($[M + Na]^+$): 1979.8198, found: 1979.8175. All the experimental results are in good agreement with the expected molecular weights and structures (see ESI†). In summary, the synthesized **MonoAzo-POSS**, **BisAzo-POSS** and **TriAzo-POSS** are in good accordance with their structures.

2.2 Thermal properties of AzoMs, MonoAzo-POSS, BisAzo-POSS and TriAzo-POSS

Fig. 6 shows TGA and DTG curves of **AzoM**s and **MonoAzo-POSS**, **BisAzo-POSS** and **TriAzo-POSS**. Obviously, there are

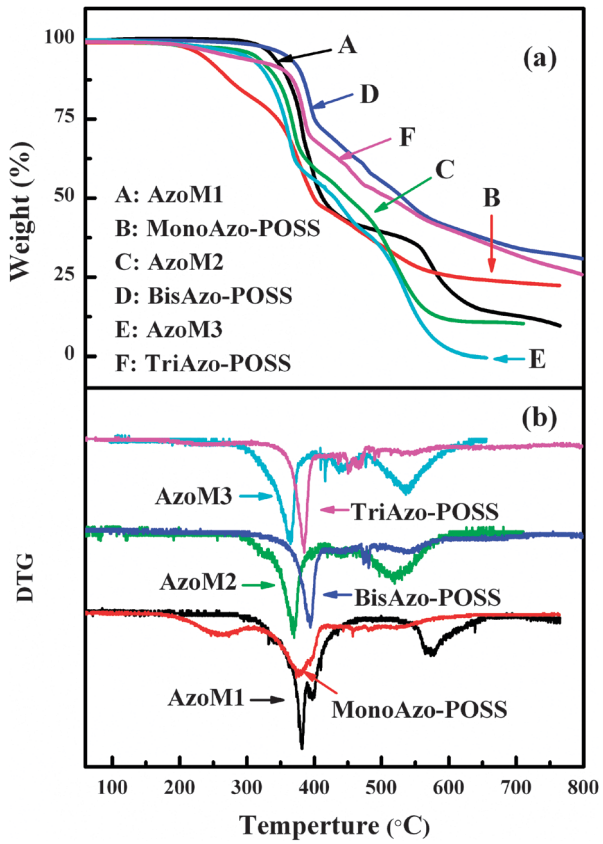

Fig. 6 TGA (a) and DTG (b) curves of **AzoMs**, **MonoAzo-POSS**, **BisAzo-POSS** and **TriAzo-POSS**.

three designated, respectively, as T_{max1}, T_{max2} and T_{max3}. They are related to T_{max}'s of the cleavage of N=N bonds, the degradation of carboxyphenyl groups, and the breakdown of the backbone.[28] And **MonoAzo-POSS**, **BisAzo-POSS** and **TriAzo-POSS** show the different thermal decomposition behaviors with **AzoM1**, **AzoM2** and **AzoM3**. Generally, the initial thermal decomposition temperature (T_d) is defined as the temperature at 5% mass loss. The above calculated values, residue yield and melting point are summarized in Table 1.

From Table 1, **AzoM1** has the highest T_d, T_{max1} and T_{max3}, and **AzoM2** shows the highest T_{max2}, which indicates that the number of azo groups affect the molecular regularity of azobenzenes, leading to their different thermal stabilities. Since the cleavage of peripheral arms (420–500 °C) and the breakdown of the Si–O–Si cage (500–700 °C) in the POSS unit are overlapped with the decompositions of carboxyphenyl groups and the azobenzene backbone,[32,33] T_d and T_{max1} values are used to compare their thermal stability. From Table 1, T_d and T_{max1} of **MonoAzo-POSS** are, respectively, 234 and 261 °C, lower than 340 and 383 °C of **AzoM1**, indicating that the stability of **MonoAzo-POSS** is poorer than that of **AzoM1**. However, **BisAzo-POSS** and **TriAzo-POSS** have better stability than **AzoM2** and **AzoM3**. These results confirm that the thermal stability of the hybrids with POSS is dominated by the following two factors. On the one hand, the incorporation of the inorganic POSS unit restricts the molecular motion,[23,34] increases the heat capacity and provides a barrier to further heat attack,[35,36] leading to high thermal stability. On the other hand, the incorporation of the inorganic POSS unit also destroys the molecular ordering structure of azobenzenes and decreases the molecular package density, leading to poor thermal stability.[37] As shown in Scheme 1, **AzoM1** is most symmetrical, and there exist binary intermolecular hydrogen bonds,[38] leading to high molecular package density, which is confirmed by its high decomposition temperature and melting point. After two or three azo groups are introduced in azobenzenes, the regularity of **AzoM2** and **AzoM3** is destroyed, leading to lower decomposition temperature and melting point than those of **AzoM1**. Especially, the steric hindrance of the POSS unit is higher than that of azo groups, and the POSS unit acts as an inert diluent to decrease the self-association interaction of molecules,[39,40] which leads to the lowest decomposition temperature and melting point of **MonoAzo-POSS**. For **BisAzo-POSS** and **TriAzo-POSS**, their T_d and T_{max1} values increase to (368, 300 °C) and (394, 385 °C) from (310, 265 °C) and (368, 363 °C) of **AzoM2** and **AzoM3**, indicating that the incorporation of POSS units effectively improves the thermal stability of **BisAzo-POSS** and **TriAzo-POSS** due to the enhanced molecular regularity and restriction effects of POSS units on molecular motion.

To understand the effect of molecular structure on the packing arrangement, the XRD patterns of **AzoM1**, **AzoM2**, **MonoAzo-POSS** and **BisAzo-POSS** (Fig. 7) were measured at room temperature. For **AzoM1**, there exist multiple sharp peaks with the four-order diffraction at $2\theta = 1.72°$, 3.41°, 5.09° (overlapping with a peak at 5.33°) and 7.11°, corresponding to a layer spacing of 5.13 nm. While the three-order diffraction at $2\theta = 5.33°$, 10.64° and 15.20° characterizes another layer spacing of 1.66 nm of **AzoM1**. The two peaks at $2\theta = 20.58°$ ($d = 0.43$ nm) and 24.37° ($d = 0.37$ nm) are ascribed to the packing of azo units and the typical π–π stacking of aryl units, respectively.[41–43] And the diffraction peak at $2\theta = 19.20°$ ($d = 0.46$ nm) is attributed to the close-packing of the alkyl chains.[43,44] These results illustrate that **AzoM1** has a high-ordered layered structure. For **AzoM2**, the

Table 1 Thermal stability of **AzoMs** and their hybrids with POSS

Compounds	T_d/°C	T_{max1}/°C	T_{max2}/°C	T_{max3}/°C	Residue yield (%)	Melting point/°C
AzoM1	340	383	401	575	9.60	~[a]
MonoAzo-POSS	234	261	375	481	22.40	165–167
AzoM2	310	368	442	518	9.74	183–185
BisAzo-POSS	368	394	478	540	31.00	184–185
AzoM3	265	363	436	538	0.01	158–159
TriAzo-POSS	300	385	456	539	26.10	175–177

[a] Melting point of **AzoM1** is close to its decomposition temperature.

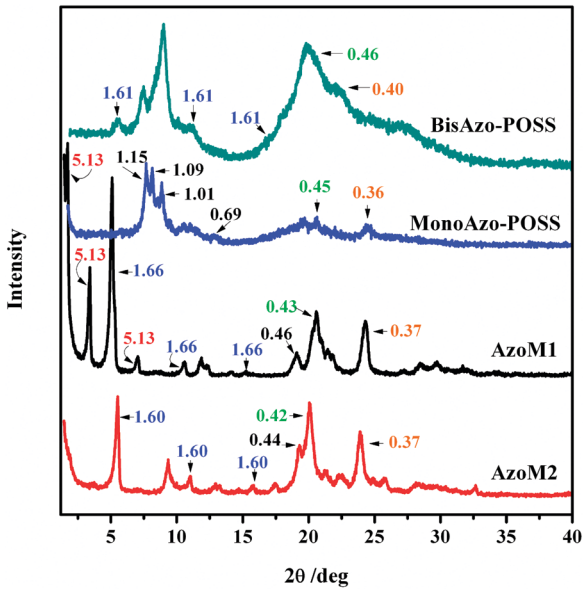

Fig. 7 XRD patterns of **AzoM1**, **AzoM2**, **MonoAzo-POSS** and **BisAzo-POSS**.

diffraction peaks of azo units (2θ = 20.11°, d = 0.44 nm), the π–π stacking of aryl units (2θ = 23.89°, d = 0.37 nm), the close-packing of the alkyl chains (2θ = 21.28°, d = 0.42 nm) are similar to those in **AzoM1**. However, **AzoM2** only has three-order diffraction at 2θ = 5.53°, 11.02° and 15.96° corresponding to a layer spacing of 1.60 nm. The results confirm that **AzoM2** exhibits lower ordering than that of **AzoM1**. Additionally, for **MonoAzo-POSS**, the peak at 2θ = 8.12° (d = 1.09 nm) reflects the size of POSS units,[45] and the peaks at 2θ = 7.67° (d = 1.15 nm), 8.83° (d = 1.01 nm), 12.9° (d = 0.69 nm), 19.6° (d = 0.45 nm) and 24.4° (d = 0.36 nm) are related to the rhombohedral crystal structure of POSS.[43,45,46] However, the diffraction peaks of azo units (2θ = 20.58°, d = 0.43 nm) and the π–π stacking of aryl units (2θ = 24.39°, d = 0.37 nm) in **MonoAzo-POSS** are weaker and broader than those in **AzoM1**, and the periodic peaks with multi-order diffraction disappear. These results confirm that the incorporation of POSS destroys the symmetry of **AzoM1** and decreases the molecular package density of **MonoAzo-POSS**. Interestingly, it can be seen that there exist the enhanced diffraction peaks of azo units at 2θ = 19.51° (d = 0.46 nm) and the π–π stacking of aryl units at 2θ = 22.41° (d = 0.40 nm), and the three-order diffraction at 2θ = 5.48°, 11.05° and 16.51° (overlapping with the peak at 19.51°) corresponding to a layer spacing of 1.61 nm in **BisAzo-POSS**. The results indicate that **BisAzo-POSS** has higher ordering than **MonoAzo-POSS**.

To further substantiate the above XRD results, the optimized geometries of **AzoM1**, **AzoM2**, **MonoAzo-POSS** and **BisAzo-POSS** were calculated by molecular modeling software (Hyper-Chem 7.5). Fig. 8 shows their energy-minimized structures. The calculated van der Waals chain length (l) of **AzoM1** is 2.45 nm. Due to the binary intermolecular hydrogen bonds, **AzoM1** exists as a dimer with a layer spacing length (d) as shown in Fig. 9. Obviously, d is double the length of l (4.90 nm) and binary hydrogen bonds, and close to the layer spacing of 5.13 nm obtained by XRD. Additionally, the calculated interplanar spacing lengths of **AzoM1** and **AzoM2** are 1.56 nm (see Fig. 8A and B), close to the above 1.66 nm and 1.60 nm determined by XRD, which suggests that **AzoM1** and **AzoM2** are lamellar (see Fig. 9A and B). As shown in Fig. 8C, the azo units in **MonoAzo-POSS** are bent towards POSS *via* the flexible –O(CH$_2$)$_6$O– spacer, the formed large steric hindrance limits the packing of **MonoAzo-POSS** as shown in Fig. 9C, leading to the weak diffraction peaks of azo and aryl units. However, different from those in **MonoAzo-POSS**, azo and aryl units in **BisAzo-POSS** unfold as shown in Fig. 8D, and they easily form an effective packing as shown in Fig. 9D.

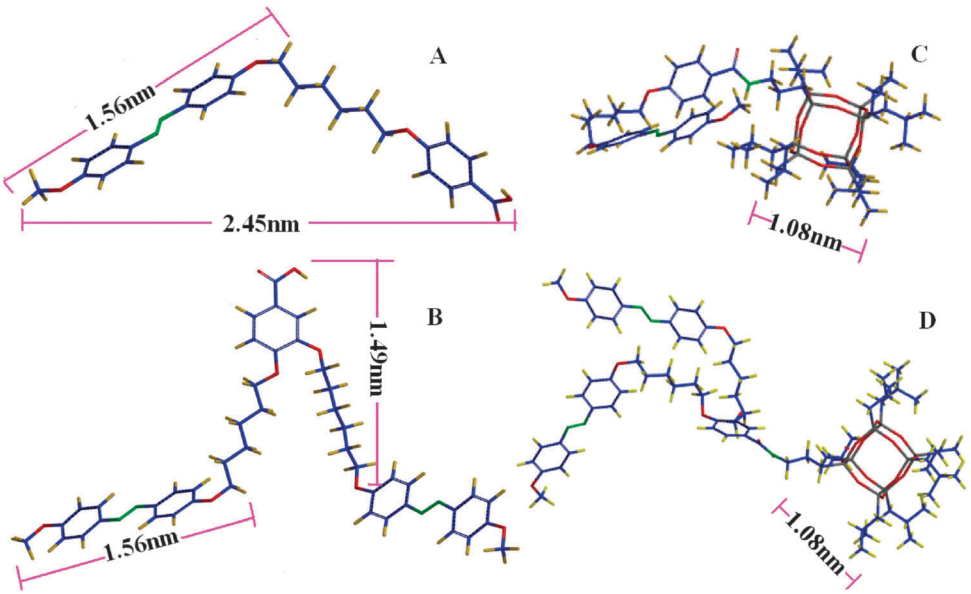

Fig. 8 Energy-minimized structures of **AzoM1** (A), **AzoM2** (B), **MonoAzo-POSS** (C) and **BisAzo-POSS** (D).

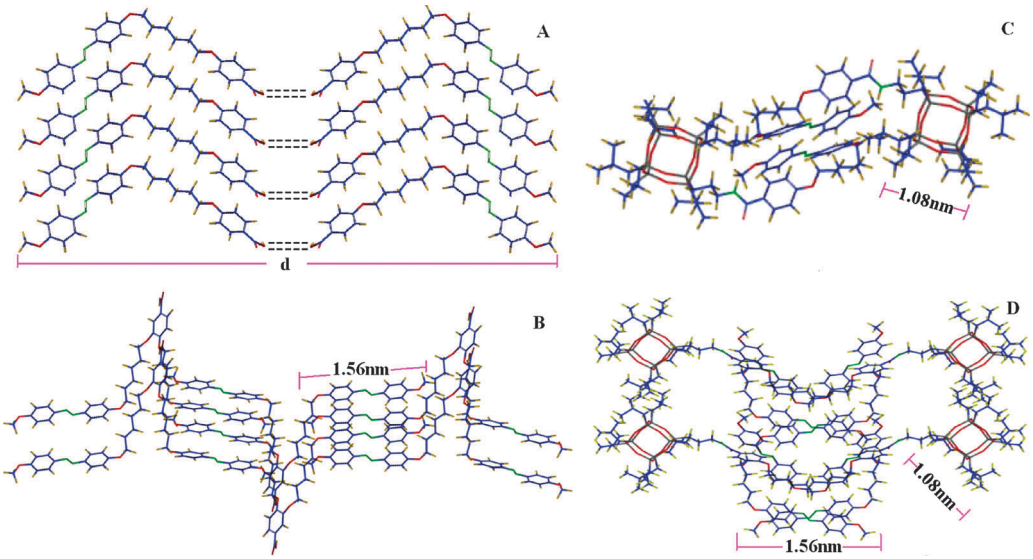

Fig. 9 Possible aggregation models of **AzoM1** (A), **AzoM2** (B), **MonoAzo-POSS** (C) and **BisAzo-POSS** (D).

2.3 Photochemical behaviors

To examine the photochemical *trans–cis* isomerization of **AzoM**s and their hybrids, their solutions in DMF were irradiated with 365 nm unpolarized UV light until they reached a photostationary state. Typically, Fig. 10 shows the changes in UV-vis spectra of **AzoM3** and **TriAzo-POSS** with different irradiation times. The absorption peaks at 360, 310 and 460 nm are, respectively, related to the π–π* transition of *trans*-azobenzene units, the π–π* and n–π* transition of the *cis*-isomer. Under UV irradiation, the absorbance at 360 nm decreases significantly while the absorbances at 310 and 460 nm increase slightly due to *trans–cis* photoisomerization. **AzoM1**, **AzoM2**, **MonoAzo-POSS** and **BisAzo-POSS** show similar features.

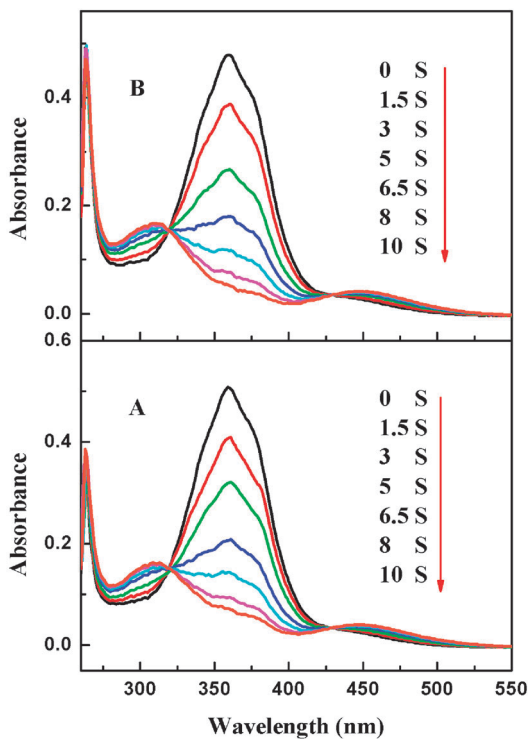

Fig. 10 UV-vis spectra of **AzoM3** (A) and **TriAzo-POSS** (B) in DMF upon irradiation with 365 nm UV light at room temperature. Arrows indicate changes upon irradiation.

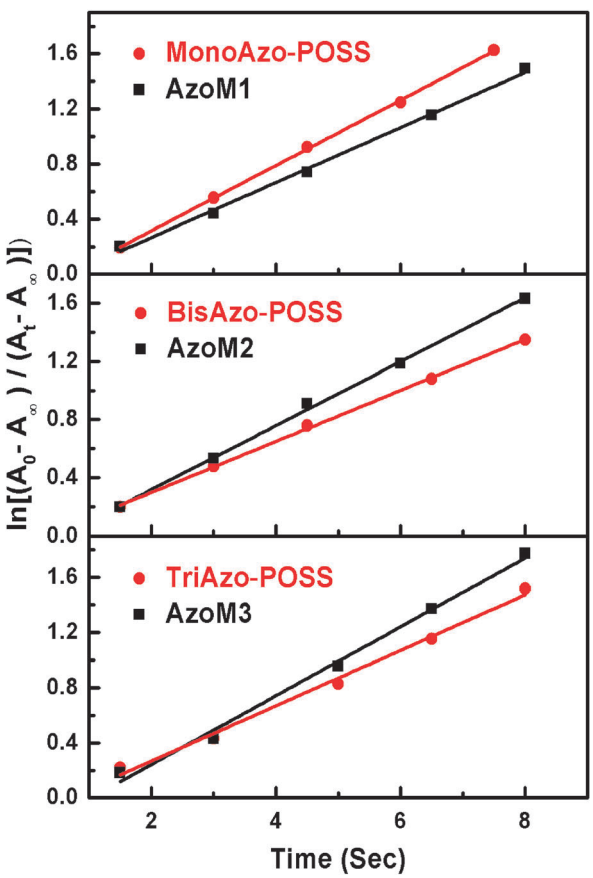

Fig. 11 $\ln[(A_0 - A_\infty)/(A_t - A_\infty)]$-$t$ plots of **AzoM**s and their hybrids with POSS.

Table 2 Photoisomerization rates of **AzoM**s and their hybrids with POSS

Compounds	**AzoM1**	**MonoAzo-POSS**	**AzoM2**	**BisAzo-POSS**	**AzoM3**	**TriAzo-POSS**
k/s^{-1}	0.20	0.24	0.22	0.17	0.25	0.20

The first-order rate constant (k) is determined by fitting the experimental data to the following equation:[13,47]

$$\ln\frac{A_0 - A_\infty}{A_t - A_\infty} = kt$$

where A_t, A_0, and A_∞ are absorbances at 360 nm at time t, time zero, and infinite time, respectively.

Fig. 11 shows the relationship between $\ln[(A_0 - A_\infty)/(A_t - A_\infty)]$ and t. Obviously, their *trans–cis* isomerizations obey the first-order reaction, the corresponding k values are listed in Table 2.

From Table 2, the k value of **AzoM1** (0.20 s^{-1}) is smaller than those of **AzoM2** (0.22 s^{-1}) and **AzoM3** (0.25 s^{-1}), indicating that the low molecular ordering of azobenzene endows azo moieties with large free volume and high mobility, and their *trans–cis* photoisomerization rates increase accordingly. Similarly, the incorporation of POSS units also decreases the molecular ordering of azobenzene, leading to the fast photoisomerization rate (0.24 s^{-1}) of **MonoAzo-POSS**. However, as discussed above, the azo moieties in **BisAzo-POSS** and **TriAzo-POSS** unfold, leading to small free volume for their mobility. Additionally, POSS units also limit their mobility, the k values of the **BisAzo-POSS** and **TriAzo-POSS** decrease to 0.17 and 0.20 s^{-1} accordingly. These results indicate that the photoisomerization of azobenzenes can be effectively controlled by their molecular structure.

3. Conclusions

The thermal stability and photoisomerization of azobenzenes could be effectively controlled by their molecular structure. The large steric hindrance of POSS destroys the molecular ordering of **AzoM1**, limits the molecular packing and offers azo moieties with a large free space, leading to poor thermal stability and high *trans–cis* photoisomerization of **MonoAzo-POSS**. But, the incorporation of POSS units does not impact on the regularity of azobenzenes obviously, and the hindrance effect of nanosize POSS on the molecular motion plays a main role in increasing the high thermal stability of **BisAzo-POSS** and **TriAzo-POSS**. Their photoisomerization rates decrease due to the steric hindrance of POSS and the unfolding structure of the azo moieties in **BisAzo-POSS** and **TriAzo-POSS**.

4. Experimental section

4.1 Materials and methods

Materials. Isobutyltrimethoxysilane ($(CH_3)_2CHCH_2Si(OCH_3)_3$) (Alfa Aesar 98%) was used without further purification. Absolute ethanol was dried by sodium, and dimethylformamide (DMF) was purified by vacuum distillation before use. Sulfuric acid (98%), nitric acid (67%), hydrochloric acid (36.5%), thionyl chloride, phenol, 4-methoxyaniline, potassium carbonate, sodium nitrite, 1,6-dibromohexane, sodium hydroxide, lithium hydroxide, absolute methanol, petroleum ether, acetone, anhydrous magnesium sulfate, chloroform, dichloromethane, ethyl acetate, tetrahydrofuran, dimethyl sulfoxide, and other chemicals were used as received from Sinopharm Group Chemical Reagent Co., Ltd, Shanghai, China.

Measurements. Fourier transform infrared (FT-IR) spectra were recorded on a Bruker Equinox 55 spectrometer with a disc of KBr. ^{1}H NMR and ^{13}C NMR spectra were recorded on a Bruker AV400 spectrometer with TMS as an internal standard. Electrospray ionization high-resolution mass spectroscopy (ESI-HRMS) was carried out on a Perkin-Elmer QSTAR mass spectrometer, fast atom bombardment mass spectrometry (FAB-MS) was carried out on a Finnigan SSQ-710 mass spectrometer. Thermal gravimetric analysis (TGA) was conducted on a TGA-7 Perkin-Elmer calorimeter under argon flow (20 mL min^{-1}) at 10 °C min^{-1}. X-Ray diffraction (XRD) was performed using an X'Pert PRO powder diffractometer with CuKα radiation (0.15406 Å) with the 2θ range of 1–40° at room temperature. UV-vis absorption spectra were recorded at room temperature in DMF solution on a diode-array spectrophotometer (Shimadzu UV-2550). The spectral region 550–280 nm was examined by using a cell path length of 10 mm. Photoisomerization experiments were carried out by using 365 nm light from an ultraviolet lamp (32 W, ELC-500, light exposure system electrolite corporation, US). Melting point data were collected on a WRS-1A Melting-point Apparatus with a heating rate of 1° min^{-1}. Calculations were made utilizing the Spartan program. This calculation package provides optimized geometries constructed by using the semi-empirical quantum chemistry AM1 method.

4.2 Synthesis

4-Hydroxy-4′-methoxyazobenzene (**HMAB**) was synthesized according to a method similar to that of ref. 28 and 29. Yield: 76.98%. IR (KBr, cm^{-1}), 3324 (υ, O–H), 3100–3050 (υ, C–H, aromatic), 2980–2850 (υ, C–H, CH_2, and CH_3), 1602–1470 (υ, C=C, aromatic), 1247–1040 (υ, C–O). 1395 (υ, N=N), and 1383 (δ, C–H, CH_2, and CH_3), 842 (δ_{oop}, p-Ar).

Synthesis of **BrMAB**. **HMAB** (11.4 g, 0.05 mol), 1,6-dibromohexane (73.2 g, 0.30 mol), and anhydrous potassium carbonate (22.175 g, 161 mmol) were added to acetone (500 mL) under magnetic stirring, and the reaction mixture was heated to 75 °C and refluxed for 36 h. After the reaction was complete, the hot solution was immediately filtered and the inorganic residues were washed thoroughly with hot acetone. The filtrates were collected and distilled under vacuum to remove acetone, and the remaining concentrated extracts were poured into cooled petroleum ether (60–90 °C). The precipitated product was filtered off and washed twice with petroleum ether to yield 13.7 g of yellow squamose crystals. Yield: 70%.

IR (KBr, cm^{-1}) 3100–3050 (υ, C–H, aromatic), 2936–2863 (υ, C–H, CH_2, and CH_3), 1602–1470 (υ, C=C, Ar), 1395 (υ, N=N), 1247–1040 (υ, C–O). 842 (δ_{oop}, p-Ar), ^{1}H NMR (400 MHz, $CDCl_3$) δ: 3.91 (s, –OCH_3, 3H), 7.01 (dd, Ar–H, 4H, *ortho* to O), 7.88 (dt, Ar–H, 4H, *ortho* to N), 4.02 (t, –OCH_2–, 2H), 1.93 (m, –OCH$_2$$CH_2$–, 2H), 1.6 (m, –$CH_2$$CH_2$–, 4H), 1.84 (m, –$CH_2CH_2$Br, 2H), 3.45 (t, –$CH_2$Br, 2H). Its FT-IR and ^{1}H NMR spectra are shown in Fig. S1 and S2 (ESI†).

Synthesis of ester of **AzoM1**. The alkyloxylation reaction was carried out by refluxing methyl-4-hydroxybenzoate (0.76 g, 5 mmol), **BrMAB** (2.346 g, 6 mmol), K_2CO_3 (0.828 g, 6 mmol), and KI (0.166 g, 1 mmol) in 2-butanone (150 mL), and the reaction mixture was stirred at 75 °C for 24 h. After the reaction, the mixed solution was concentrated *in vacuo*, and the residue was poured into dilute HCl. The yellow precipitate was filtered, and washed with water until the liquid phase became neutral and dried *in vacuo* to afford a yellow solid. The crude product was recrystallized from $CHCl_3$ and dried under vacuum to get 1.80 g of a yellow powder. Yield: 97.3%. IR (KBr, cm^{-1}), 2936–2864 (υ, C–H, CH_2, and CH_3), 1652 (υ, C=O), 1601–1468 (υ, C=C, Ar), 1246–1028 (υ, C–O). 1395 (υ, N=N), 842 (δ_{oop}, p-Ar), ^{1}H NMR (400 MHz, $CDCl_3$) δ: 3.87 (s, –OCH_3, 6H), 6.95 (dd, Ar–H, 4H, *ortho* to O), 7.86 (m, Ar–H, 4H, *ortho* to N), 4.08 (t, –OCH_2–, 4H), 1.84 (m, –OCH$_2$$CH_2$–, 4H), 1.59 (m, –$CH_2$$CH_2$–, 4H), 6.88 (dd, Ar–H, 2H, *ortho* to O), 7.99 (dd, Ar–H, 2H, *ortho* to COOCH$_3$). Its ^{1}H NMR spectrum is shown in Fig. S3 (ESI†).

Synthesis of esters of **AzoM2** and **AzoM3**. Esters of **AzoM2** and **AzoM3** were synthesized according to the synthesis of **AzoM1**. Yield for esters of **AzoM2**: 98.4%. 2935–2860 (υ, C–H, CH_2, and CH_3), 1686 (υ, C=O), 1601–1467 (υ, C=C, Ar), 1246–1028 (υ, C–O). 1392 (υ, N=N), 842 (δ_{oop}, p-Ar). Yield for ester of **AzoM3**: 99.35%.

Synthesis of AzoM1. To a solution of ester of **AzoM1** (2.31 g, 5 mmol) in 250 mL of the EtOH/THF mixture was added a solution of NaOH (4 g, 100 mmol) in deionized water (100 mL), and the reactants was stirred and refluxed for 8 h. The mixed solution was concentrated *in vacuo*. The residues were poured into dilute HCl at 0 °C, and the reaction mixture was acidified to pH < 7 with aqueous HCl solution. The yellow precipitate was filtered and washed with water until the liquid phase became neutral. After drying, the crude product was recrystallized from $CHCl_3$ and dried *in vacuo* to get 1.97 g of **AzoM1** as a yellow powder. Yield 87.9%. No NMR spectrum was recorded because the solubility of the final compound was too low for ordinary solvents ($CDCl_3$, CD_3OD, $(CD_3)_2CO$, DMSO and so on). IR (KBr, cm^{-1}), 3313 (υ, O–H), 2936–2864 (υ, C–H, CH_2, and CH_3), 1656 (υ, C=O), 1601–1468 (υ, C=C, Ar), 1246–1029 (υ, C–O). 1395 (υ, N=N), 842 (δ_{oop}, p-Ar). Its FT-IR spectrum is shown in Fig. S4 (ESI†).

Synthesis of AzoM2. Following the procedure for **AzoM1**, **AzoM2** was obtained from an ester of **AzoM2** under reflux for 12 h. The crude product was purified using silica gel column chromatography eluting with CH_2Cl_2/MeOH (15/1) to give **AzoM2** as a yellow powder (3.2 g, yield: 82.7%). IR (KBr, cm^{-1}), 3448 (υ, O–H), 2935–2857 (υ, C–H, CH_2, and CH_3), 1684 (υ, C=O), 1601–1467 (υ, C=C, Ar), 1246–1029 (υ, C–O). 1392 (υ, N=N), 842 (δ_{oop}, p-Ar), ^{1}H NMR (400 MHz, Pr–d_5) δ: 3.75 (s, –OCH_3, 6H), 7.13 (d, Ar–H, 8H, *ortho* to O), 8.15 (d, Ar–H, 8H, *ortho* to N), 4.05 (t, –OCH_2–, 4H), 3.95 (t, –CH_2O–, 4H) 1.90 (m, –OCH$_2$$CH_2$–, 8H), 1.48 (m, –$CH_2$$CH_2$–, 8H), 8.15 (d, Ar–H, 1H,), 8.2 (d, Ar–H, 1H), 7.2 (d, Ar–H, 1H). Its FT-IR and ^{1}H NMR spectra are shown in Fig. S5 and S6 (ESI†).

Synthesis of AzoM3. AzoM3 was obtained as an orange powder, in a similar procedure as described for the synthesis of **AzoM1** reflux for 20 h. The crude product was purified by silica gel column chromatography eluting with CH_2Cl_2/MeOH (20/1) to give 3.685 g of **AzoM3**. Yield: 67% IR (KBr, cm^{-1}), 3449 (υ, O–H), 2937–2861 (υ, C–H, CH_2, and CH_3), 1684 (υ, C=O), 1596–1465 (υ, C=C, Ar), 1248–1028 (υ, C–O). 1391 (υ, N=N), 840 (δ_{oop}, p-Ar), ^{1}H NMR (400 MHz, Pr–d_5) δ: 3.85 (s, –OCH_3, 9H), 6.95 (d, Ar–H, 12H, *ortho* to O), 7.83 (d, Ar–H, 12H, *ortho* to N), 4.07 (t, –OCH_2–, 6H), 3.99 (t, –CH_2O–, 6H) 1.83 (m, –OCH$_2$$CH_2$–, 12H), 1.77 (m, –$CH_2$$CH_2$–, 12H), 7.34 (d, Ar–H, 2H). Its FT-IR and ^{1}H NMR spectra are shown in Fig. S7 and S8 (ESI†).

Synthesis of trisilanolisobutyl-POSS. Isobutyltrimethoxysilane (46.65 g, 261.6 mmol), acetone (250 mL), distilled water (4 g, 222 mmol), and LiOH·H_2O (5.0 g, 119.1 mmol) were charged in a three-necked flask equipped with a reflux condenser and a magnetic stirrer. The mixture was refluxed in an oil bath for 20 h with vigorous stirring and was acidified by quenching it into 1 mol L^{-1} HCl (aq) (250 mL) and stirring for 2 h. The resulting solid was filtered and washed two times with CH_3CN (2 × 80 mL) and air dried. 32.36 g of the product was isolated in 73.8% yield. IR (KBr, cm^{-1}), 3250 (υ, O–H), 2955–2872 (υ, C–H, CH_2, and CH_3), 1111 (υ, Si–O). Its FT-IR spectrum is shown in Fig. S9 (ESI†).

Synthesis of NH_2-POSS. Trisilanolisobutyl-POSS (20 g, 25.20 mmol) was dissolved in ethanol (125 mL) followed by addition of 3-aminopropyltrimethoxysilane (4.35 g, 25.20 mmol) and tetraethylammonium hydroxide (0.39 g, 0.52 mmol of a 20% methanol solution). The solution was stirred at 20 °C for 36 h. The solvent was evaporated and the product was washed with acetonitrile, recovered, and dried to yield 17.1 g, 77.4% of the product as a white solid. IR (KBr, cm^{-1}), 3567–3503 (υ, N–H), 2956–2873 (υ, C–H, CH_2, and CH_3), 1112 (υ, Si–O), ^{1}H NMR (400 MHz, $CDCl_3$) δ: 2.6 (s, –$CH_2$$NH_2$, 2H), 1.9 (m, –$CH_2$$CH$, –$CH_2$$CH_2$, 9H), 0.6 (t, Si–$CH_2$–, 16H), 1.0 (d, –CH($CH_3$)$_2$, 42H), 7.1 (d, –$NH_2$, 2H). Its FT-IR spectrum is shown in Fig. S10 (ESI†).

Synthesis of **AzoCOCl1**, **AzoCOCl2** and **AzoCOCl3**. It should be noted that the acyl chlorides were induced on **AzoCOCl1**, **AzoCOCl2** and **AzoCOCl3** by reaction of **AzoM1**, **AzoM2** and **AzoM3** with excess thionyl chloride ($SOCl_2$), respectively. Typically for **AzoCOCl1**, **AzoM1** (1.12 g, 2.5 mmol) was suspended in 50 mL of CH_2Cl_2 and a catalytic amount of DMF was added, and then $SOCl_2$ (0.893 g, 7.38 mmol) was added dropwise under stirring. The reaction was carried out for 4 h at room temperature, and at 40 °C for

another 4 h under reflux conditions till the reactant became a clear homogenous solution. Then CH_2Cl_2 and the excessive $SOCl_2$ were evaporated under vacuum carefully. The resulting orange acyl chloride was dissolved in 80 mL of CH_2Cl_2. **AzoCOCl2** and **AzoCOCl3** were synthesized by the same procedure as described for the preparation of **AzoCOCl1**.

Synthesis of **MonoAzo-POSS**. A three-neck 50 mL flask was charged with **NH_2-POSS** (1.746 g, 2 mmol), CH_2Cl_2 (10 mL) and triethylamine (0.40 mL, 2.86 mmol) in order and cooled to 0 °C with stirring. The acyl chloride solution (**AzoCOCl1**) was added into chilled amine solution; the flask containing the acyl chloride was treated with an additional 5 mL of CH_2Cl_2 and again added into the amine solution. The resulting mixture was allowed to stir for 2 h at 0 °C, and then refluxed for another 4 h. The light brown phase was washed with sat. aq. $NaHCO_3$ (5 × 100 mL), distilled water (3 × 100 mL), dried ($MgSO_4$), filtered and concentrated under reduced pressure to get a yellow solid. The crude product was purified using silica gel column chromatography eluting with CH_2Cl_2/MeOH (30/1) to give **MonoAzo-POSS** as a yellow powder (1.59 g, 61%). IR (KBr, cm^{-1}), 3289 (υ, N–H), 2955–2871 (υ, C–H, CH_2, and CH_3), 1109 (υ, Si–O), 1636 (υ, C═O), 1604–1469 (υ, C═C, Ar), 1401 (υ, N═N), 1254–1170 (υ, C–O), 840 (δ_{00P}, p-Ar), ^{1}H NMR (400 MHz, $CDCl_3$) δ: 3.89 (s, –OCH_3, 3H), 6.98 (dd, Ar–H, 4H, *ortho* to O), 7.88 (m, Ar–H, 4H, *ortho* to N), 4.08 (t, –OCH_2–, 4H), 1.84 (m, –OCH$_2$CH_2–, –SiCH$_2$CH, 11H), 1.58 (m, –CH_2CH_2–, 4H), 6.89 (dd, Ar–H, 2H, *ortho* to O), 7.70 (dd, Ar–H, 2H, *ortho* to CONH–), 5.99 (s, *NH*, 1H), 3.42 (t, –NHCH_2, 2H), 1.69 (m, –NHCH$_2$CH_2, 2H), 0.64 (m, –SiCH_2, CH_2, –2H), 0.59 (m, –SiCH_2, CH, –14H), 0.98 (D, –CH(CH_3)$_2$, –42H), ^{13}C NMR (400 MHz, $CDCl_3$,), δ 166.98 (C═O), 114.69 (*o*-ArC to –OCH$_3$), 114.20 (*o*-ArC to –O(CH$_2$)$_6$–), 124.36 (*m*-ArC to –OCH$_3$ and –O(CH$_2$)$_6$–), 147.07 (*p*-ArC to –OCH3), 146.95 (*p*-ArC to –O(CH$_2$)$_6$–), 161.61 (ArC next to –OCH$_3$ and next to –O(CH$_2$)$_6$–), 161.17 (*p*-ArC to –CONH–), 131.59 (*o*-ArC to –CONH–), 128.57 (*m*-ArC to –CONH–), 127.07 (ArC next to –CONH–), 42.23 (NCH$_2$(CH$_2$)$_2$), 25.70 (SiCH$_2$CH(CH$_3$)$_2$), 23.86 (SiCH$_2$CH-(CH$_3$)$_2$), 23.14 (NCH$_2$CH$_2$CH$_2$), 22.52 (SiCH$_2$CH(CH$_3$)$_2$), 9.52 (N(CH$_2$)$_2$CH$_2$), 55.57 (–OCH$_3$), 68.13, 68.00 (–OCH$_2$(CH$_2$)$_4$CH$_2$O–), 29.17 (–OCH$_2$CH$_2$(CH$_2$)$_2$CH$_2$-CH$_2$O–), 29.12 (–O(CH$_2$)$_2$CH$_2$CH$_2$(CH$_2$)$_2$O–), FAB-MS, m/z(%): 1304.7 ([M + H]$^+$). Its FT-IR, ^{1}H NMR, ^{13}C NMR and FAB-MS spectra are shown in Fig. S11 and S14 (ESI†).

Synthesis of **BisAzo-POSS** and **TriAzo-POSS**. **BisAzo-POSS** and **TriAzo-POSS** were obtained as orange powder *via* a similar procedure as described for the synthesis of **MonoAzo-POSS**, using **NH_2-POSS** reacted with **AzoCOCl2** and **AzoCOCl3**, respectively, and the crude products were purified using silica gel column chromatography eluting with CH_2Cl_2/MeOH (35/1) to yield **BisAzo-POSS** (1.92 g, 59%) and **TriAzo-POSS** (2.47 g, 63%). Spectra of **BisAzo-POSS**: IR (KBr, cm^{-1}), 3289 (υ, N–H), 2954–2870 (υ, C–H, CH_2, and CH_3), 1108 (υ, Si–O), 1633 (υ, C═O), 1599–1469 (υ, C═C, Ar), 1400 (υ, N═N), 1256–1167 (υ, C–O), 840 (δ_{00P}, p-Ar), ^{1}H NMR (400 MHz, $CDCl_3$) δ: 3.84 (s, –OCH$_3$, 6H), 6.97 (dd, Ar–H, 8H, *ortho* to O), 7.84 (m, Ar–H, 8H, *ortho* to N), 4.03 (t, –OCH_2–, 8H), 1.83 (m, –OCH$_2$CH_2–, –SiCH$_2$CH, 15H), 1.58 (m, –CH_2CH_2–, 8H), 6.83 (dd, Ar–H, 1H), 7.42 (dd, Ar–H, 1H), 6.01 (s, *NH*, 1H), 3.42 (t, –NHCH_2, 2H), 1.71 (m, –NHCH$_2$CH_2, 2H), 0.63 (m, –SiCH_2, CH_2, –2H), 0.59 (m, –SiCH_2, CH, –14H), 0.98(D, –CH(CH_3)$_2$, –42H), ^{13}C NMR (400 MHz, $CDCl_3$) δ: 167.07 (C═O),114.65 (*o*-ArC to –OCH$_3$), 114.15 (*o*-ArC to –O(CH$_2$)$_6$–), 124.34 (*m*-ArC to –OCH$_3$ and –O(CH$_2$)$_6$–), 146.98 (*p*-ArC to –OCH3), 146.95 (*p*-ArC to –O(CH$_2$)$_6$–), 161.54 (ArC next to –OCH$_3$), 161.15 (ArC next to –O(CH$_2$)$_6$–), 119.15, 112.3 (*o*-ArC to –CONH–), 151.74 (*p*-ArC to –CONH–), 149.00 (*m*-ArC (next to –O(CH$_2$)$_6$–) to –CONH–), 113.01 (*m*-ArC to –CONH–), 127.60 (ArC next to –CONH–), 42.32 (NCH$_2$(CH$_2$)$_2$), 25.82 (SiCH$_2$CH(CH$_3$)$_2$), 23.85 (SiCH$_2$CH(CH$_3$)$_2$), 23.15 (NCH$_2$-CH$_2$CH$_2$), 22.48 (SiCH$_2$CH(CH$_3$)$_2$), 9.53 (N(CH$_2$)$_2$CH$_2$), 55.50 (–OCH$_3$), 68.98, 68.14 (–OCH$_2$(CH$_2$)$_4$CH$_2$O–), 29.69 (–OCH$_2$CH$_2$(CH$_2$)$_2$CH$_2$CH$_2$O–), 29.10 (–O(CH$_2$)$_2$CH$_2$CH$_2$-(CH$_2$)$_2$O–), HRMS-MS calcd $C_{76}H_{119}N_5Si_8O_{19}Na$ ([M + Na]$^+$): 1653.6566, found: 1653.6621. Spectra of **TriAzo-POSS**: IR (KBr, cm^{-1}), 3289 (υ, N–H), 2951–2870 (υ, C–H, CH_2, and CH_3), 1107 (υ, Si–O), 1634 (υ, C═O), 1594–1465 (υ, C═C, Ar), 1392 (υ, N═N), 1250 (υ, C–O), 840 (δ_{00P}, p-Ar). ^{1}H NMR (400 MHz, $CDCl_3$) δ: 3.86 (s, –OCH_3, 9H), 6.97 (m, Ar–H, 14H, *ortho* to –OCH$_3$, *ortho* to –OCH_2–, *ortho* to –CONH), 7.83 (m, Ar–H, 12H, *ortho* to N), 4.00 (t, –OCH_2–, 12H), 1.84 (m, –OCH$_2$CH_2–, –SiCH$_2$CH, 19H), 1.57 (m, –CH_2CH_2–, 12H), 5.99 (s, *NH*, 1H), 3.42 (t, –NHCH_2, 2H), 1.66 (m, –NHCH$_2$CH_2, 2H), 0.65 (m, –SiCH_2, CH$_2$CH$_2$NH, 2H), 0.59 (m, –SiCH_2, CH, 14H), 0.98 (D, –CH(CH_3)$_2$, 42H), ^{13}C NMR (400 MHz, $CDCl_3$) δ: 167.29(C═O), 114.65 (*o*-ArC to –OCH$_3$), 114.16 (*o*-ArC to –O(CH$_2$)$_6$–), 124.36 (*m*-ArC to –OCH$_3$ and –O(CH$_2$)$_6$–), 146.97 (*p*-ArC to –OCH3), 146.94 (*p*-ArC to –O(CH$_2$)$_6$–), 161.54 (ArC next to –OCH$_3$), 161.13 (ArC next to –O(CH$_2$)$_6$–), 105.83 (*o*-ArC to –CONH–), 152.79 (*m*-ArC to –CONH–), 141.04 (*p*-ArC to –CONH–), 130.13 (ArC next to –CONH–), 42.52 (NCH$_2$(CH$_2$)$_2$), 25.72 (SiCH$_2$-CH(CH$_3$)$_2$), 23.92 (SiCH$_2$CH(CH$_3$)$_2$), 23.2 (NCH$_2$CH$_2$CH$_2$), 22.53 (SiCH$_2$CH(CH$_3$)$_2$), 9.59 (N(CH$_2$)$_2$CH$_2$), 55.50 (–OCH$_3$), 68.99, 68.19 (–OCH$_2$(CH$_2$)$_4$CH$_2$O–), 31.94 (–OCH$_2$CH$_2$-(CH$_2$)$_2$CH$_2$CH$_2$O–), 29.36 (–O(CH$_2$)$_2$CH$_2$CH$_2$(CH$_2$)$_2$O–), HRMS-MS calcd $C_{95}H_{141}N_7Si_8O_{22}Na$ ([M + Na]$^+$): 1979.8198, found: 1979.8175. Their FT-IR, ^{1}H NMR, ^{13}C NMR and ESI-HRMS spectra are shown in Fig. S15 and S22 (ESI†), respectively.

Acknowledgements

We wish to acknowledge the financial support by the Outstanding Youth Fund of the National Natural Science Foundation of China (50825301), and by the Fund from the State Key Laboratory of Plastic Forming Simulation and Moulding Technology at Huazhong University of Science and Technology (HUST). We thank the HUST Analytical and Testing Center for allowing us to use its facilities.

References

1 X. Tong, G. Wang, A. Yavrian, T. Galstian and Y. Zhao, *Adv. Mater.*, 2005, **17**, 370–374.
2 I. Mita, K. Horie and K. Hirao, *Macromolecules*, 1989, **22**, 558–563.
3 A. Natansohn and P. Rochon, *Chem. Rev.*, 2002, **102**, 4139–4175.

4 S. Xie, A. Natansohn and P. Rochon, *Chem. Mater.*, 1993, **5**, 403–411.
5 T. Nguyen, H.-R. Tseng, P. Celestre, A. Flood, Y. Liu, J. F. Stoddart and J. I. Zink, *Proc. Natl. Acad. Sci. U. S. A.*, 2005, **102**, 10029–10034.
6 V. Shibaev, A. Bobrovsky and N. Boiko, *Prog. Polym. Sci.*, 2003, **28**, 729–836.
7 X. Su, S. Guang, H. Xu, X. Liu, S. Li, X. Wang, Y. Deng and P. Wang, *Macromolecules*, 2009, **42**, 8969–8976.
8 Z. Q. Lu, P. Shao, J. Li, J. L. Hua, J. G. Qin, A. J. Qin and C. Ye, *Macromolecules*, 2004, **37**, 7089–7096.
9 S. Angelos, M. Liong, E. Choi and J. I. Zink, *Chem. Eng. J. (Amsterdam, Neth.)*, 2008, **137**, 4–13.
10 T. Hugel, N. B. Holland, A. Cattani, L. Moroder, M. Seitz and H. Gaub, *Science*, 2002, **296**, 1103–1106.
11 Y. Yu, M. Nakano and T. Ikeda, *Nature*, 2003, **425**, 145.
12 G. Pace, V. Ferri, C. von Grave, M. Elbing, C. Hanisch, M. Zharnikov, M. Mayor, M. A. Rampi and P. Samorì, *Proc. Natl. Acad. Sci. U. S. A.*, 2007, **104**, 9937–9942.
13 T. Sasaki, T. Ikeda and K. Ichimura, *Macromolecules*, 1993, **26**, 151–154.
14 Y. Cui, G. Qian, L. Chen, Z. Wang, J. Gao and M. Wang, *J. Phys. Chem. B*, 2006, **110**, 4105–4110.
15 P. Sierocki, H. Maas, P. Dragut, G. Richardt, F. Vogtle, L. D. Cola, F. A. M. Brouwer and J. I. Zink, *J. Phys. Chem. B*, 2006, **110**, 24390–24398.
16 M. Ueda, H.-B. Kim, T. Ikeda and K. Ichimura, *Chem. Mater.*, 1992, **4**, 1229–1233.
17 R. Y. Kannan, H. J. Salacinski, P. E. Butler and A. M. Seifalian, *Acc. Chem. Res.*, 2005, **38**, 879–884.
18 D. B. Cordes, P. D. Lickiss and F. Rataboul, *Chem. Rev.*, 2010, **110**, 2081–2173.
19 G. H. Mehl and J. W. Goodby, *Angew. Chem., Int. Ed. Engl.*, 1996, **35**, 2641–2643.
20 I. M. Saez and J. W. Goodby, *Liq. Cryst.*, 1999, **26**, 1101–1105.
21 I. M. Saez and J. W. Goodby, *J. Mater. Chem.*, 2001, **11**, 2845–2851.
22 Q. Pan, X. Chen, X. Fan, Z. Shen and Q. Zhou, *J. Mater. Chem.*, 2008, **18**, 3481–3488.
23 X. Su, S. Guang, C. Li, H. Xu, X. Liu, X. Wang and Y. Song, *Macromolecules*, 2010, **43**, 2840–2845.
24 M. Y. Lo, C. Zhen, M. Lauters, G. E. Jabbour and A. Sellinger, *J. Am. Chem. Soc.*, 2007, **129**, 5808–5809.
25 J. Miyake and Y. Chujo, *Macromol. Rapid Commun.*, 2008, **29**, 86–92.
26 M. S. Soh, A. U. J. Yap and A. Sellinger, *Eur. Polym. J.*, 2007, **43**, 315–327.
27 K. Tanaka, F. Ishiguro and Y. Chujo, *J. Am. Chem. Soc.*, 2010, **132**, 17649–17651.
28 Y. Yang, X. Wang, L. Liu, X. Xie, Z. Yang, R. Kwok, Y. Li and Y. W. Mai, *J. Phys. Chem. C*, 2007, **111**, 11231–11239.
29 T. Mitsuoka, H. Sato, J. Yoshida, A. Yamagishi and Y. Einaga, *Chem. Mater.*, 2006, **18**, 3442–3447.
30 F. J. Feher, T. A. Budzichowski, R. L. Blanski, K. J. Weller and J. W. Ziller, *Organometallics*, 1991, **10**, 2526–2528.
31 F. J. Feher, K. J. Weller and J. J. Schwab, *Organometallics*, 1995, **14**, 2009–2017.
32 D. Neumann, M. Fisher, I. Tran and J. Matisons, *J. Am. Chem. Soc.*, 2002, **124**, 13998–13999.
33 H. Liu, S. Kondo, N. Takeda and M. Unno, *J. Am. Chem. Soc.*, 2008, **130**, 10074–10075.
34 H. Xu, B. Yang, J. Wang, S. Guang and C. Li, *J. Polym. Sci., Part A: Polym. Chem.*, 2007, **45**, 5308–5317.
35 S. Sulaiman, A. Bhaskar, J. Zhang, R. Guda, T. Goodson, III and R. M. Laine, *Chem. Mater.*, 2008, **20**, 5563–5573.
36 E. Markovic, M. Ginic-Markovic, S. Clarke, J. Matisons, M. Hussain and G. P. Simon, *Macromolecules*, 2007, **40**, 2694–2701.
37 Y. Feng, Y. Jia, S. Guang and H. Xu, *J. Appl. Polym. Sci.*, 2010, **115**, 2212–2220.
38 B. Bai, H. Wang, H. Xin, B. Long and M. Li, *Liq. Cryst.*, 2007, **34**, 659–665.
39 S. Wu, T. Hayakawa, M. Kakimoto and H. Oikawa, *Macromolecules*, 2008, **41**, 3481–3487.
40 H. Y. Xu, S. W. Kuo, J. S. Lee and F. C. Chang, *Macromolecules*, 2002, **35**, 8788–8793.
41 N. Kaori, N. Shusaku and S. Takahiro, *Chem. Mater.*, 2009, **21**, 2624–2631.
42 A. Ajayaghosh and S. J. George, *J. Am. Chem. Soc.*, 2001, **123**, 5148–5149.
43 J. Miao and L. Zhu, *J. Phys. Chem. B*, 2010, **114**, 1879–1887.
44 Y. Xiong, Q. Liu, H. Wang and Y. Yang, *J. Colloid Interface Sci.*, 2008, **318**, 496–500.
45 E. Markovic, J. Matisons, M. Hussain and G. P. Simon, *Macromolecules*, 2007, **40**, 4530–4534.
46 O. Monticelli, A. Fina, A. Ullah and P. Waghmare, *Macromolecules*, 2009, **42**, 6614–6623.
47 S. L. Sin, L. H. Gan, X. Hu, K. C. Tam and Y. Y. Gan, *Macromolecules*, 2005, **38**, 3943–3948.

